LAWRENCE
LIVERMORE
NATIONAL
LABORATORY

LLNL-JRNL-423409

Discovery, SAR, and Radiolabeling of Halogenated Benzimidazole Carboxamide Antagonists as Useful Tools for (alpha)4(beta)1 Integrin Expressed on T- and B-cell Lymphomas

R. D. Carpenter, A. Natarajan, E. Y. Lau, M. Andrei, D. M. Solano, F. C. Lightstone, S. J. DeNardo, K. S. Lam, M. J. Kurth

February 10, 2010

Cancer Research

Disclaimer

Discovery, SAR, and Radiolabeling of Halogenated Benzimidazole Carboxamide Antagonists as Useful Tools for $\alpha_4\beta_1$ Integrin Expressed on T- and B-cell Lymphomas[1,2,3,4,5,6,7,8]

Richard D. Carpenter,[†] Arutselvan Natarajan,[§] Edmond Y. Lau,[£] Mirela Andrei,[‡] Danielle M. Solano,[†] Felice C. Lightstone,[£] Sally J. DeNardo,[§] Kit S. Lam,[‡] Mark J. Kurth[†]

[†]Department of Chemistry, University of California, Davis, Davis, CA 95616

[§]Division of Hematology and Oncology, and Radiodiagnosis and Therapy, Department of Internal Medicine, UC Davis Cancer Center, University of California, Davis, School of Medicine, Sacramento, CA 95817

[£]Physical and Life Sciences Directorate, Lawrence Livermore National Laboratory, Livermore, CA 94550

[‡]Division of Hematology and Oncology, Department of Internal Medicine, UC Davis Cancer Center, University of California, Davis, School of Medicine, Sacramento, CA 95817

Running Title: Halogenated benzimidazole antagonists of $\alpha_4\beta_1$ integrin

Key Words: $\alpha_4\beta_1$ integrin, benzimidazole, radiolabeling, medicinal chemistry, lymphoma

---

[1] **Grant support:** National Cancer Institute (U19CA113298), National Science Foundation (CHE-0614756), National Institute for General Medical Sciences (RO1-GM076151), American Chemical Society's Division of Medicinal Chemistry Predoctoral Fellowship sponsored by Sanofi-Aventis (R.D. Carpenter), Howard Hughes Medical Institute Med into Grad Fellowship (R.D. Carpenter), UC Davis R. B. Miller Graduate Fellowship and Outstanding Dissertation Award (R.D. Carpenter), Alfred P. Sloan Minority Ph.D. Program (D.M. Solano), and UC Davis Alliance for Graduate Education and the Professoriate Advantage Program (D.M. Solano). NMR spectrometers were in part funded by the National Science Foundation (CHE-0443516 and CHE-9808183). A portion of this work was performed under the auspices of the U.S. Department of Energy by Lawrence Livermore National Laboratory under Contract DE-AC52-07NA27344.

[2] **Requests for reprints:** Mark J. Kurth, Department of Chemistry, University of California, Davis, Davis, CA 95616. Phone: (530) 752-8192, Fax: (530) 752-8895, E-mail: mjkurth@ucdavis.edu.

[3] This research is dedicated in remembrance of our former colleague Professor Aaron D. Mills (University of Idaho).

[4] Assistance with data compilation by Gary Mirick (UC Davis Cancer Center) is duly acknowledged.

[5] Supplemental Data for this article are available at Cancer Research Online (http://cancerres.aacrjournals.org/).

[6] K.S. Lam and M.J. Kurth share senior authorship.

[7] Current address for R.D. Carpenter: Department of Biomedical Engineering, Genome and Biomedical Sciences Facility, University of California, Davis, Davis, CA 95616.

[8] Current address for A. Natarajan: Molecular Imaging Program at Stanford, Department of Radiology, Stanford University, Stanford, CA 94305-5427.

Abstract

The cell surface receptor $\alpha_4\beta_1$ integrin is an attractive yet poorly understood target for selective diagnosis and treatment of T- and B-cell lymphomas. This report focuses on the rapid microwave preparation of medicinally pertinent benzimidazole heterocycles, structure-activity relationships (SAR) of novel halobenzimidazole carboxamide antagonists **3-6**, and preliminary biological evaluation of radioiodinated agents **7**, **8**, and **18**. The I-125 derivative **18** had good tumor uptake (12 $\pm$ 1% ID/g at 24 h; 4.5 $\pm$ 1% ID/g at 48 h) and tumor:kidney ratio (~4:1 at 24 h; 2.5:1 at 48 h) in xenograft murine models of B-cell lymphoma. Molecular homology models of $\alpha_4\beta_1$ integrin have predicted that docked halobenzimidazole carboxamides have the halogen atom in a suitable orientation for halogen-hydrogen bonding. These high affinity (~ pM binding) halogenated ligands are attractive tools for medicinal and biological use; the fluoro and iodo derivatives are potential radiodiagnostic (^{18}F) or radiotherapeutic (^{131}I) agents, whereas the chloro and bromo analogues could provide structural insight into integrin-ligand interactions through photoaffinity cross-linking/mass spectroscopy experiments, as well as co-crystallization X-ray studies.

Introduction

Current cancer chemotherapeutic agents aim to annihilate tumors through mechanisms such as DNA alkylation, unnatural base-pair recognition, inhibition of topoisomerases, and microtubule stabilization mechanisms. However, these agents, have a narrow therapeutic index, are administered near their maximum tolerated dose (MTD), and are largely non-discriminatory in recognizing either normal or cancerous cells. As a consequence, patients suffer from serious side effects including neutropenia, thrombocytopenia, neuropathy, nausea, vomiting, diarrhea, hair loss, anemia, and various organ toxicities. While significant effort has been directed through lengthy syntheses of complex cytotoxic natural products, it is not until recent years that attention has been focused towards target-selective chemotherapeutics that could reduce off-target binding and ensuing side effects (1).

The resting or activated conformations of $\alpha_4\beta_1$ integrin allow for the application of target-selective agents for malignant lymphoid cancers; activated $\alpha_4\beta_1$ integrin is expressed on leukemias, lymphomas, melanomas, and sarcomas (2,3). Integrins are heterodimeric transmembrane receptor proteins crucial for cell-cell, cell-matrix, and cell-pathogen interactions (4). Integrin $\alpha_4\beta_1$ plays an important role in autoimmune diseases and inflammation (5), as well as tumor growth, angiogenesis, and metastasis (6-11). Indeed, $\alpha_4\beta_1$ integrin facilitates tumor cell extravasation (6), prevents apoptosis of malignant B-chronic lymphocytic leukemia cells (7), is key to drug resistance in both multiple myeloma and acute myelogenous leukemia (8), and has been selectively targeted with peptidomimetics (3, 13-17). Nonetheless, $\alpha_4\beta_1$ integrin has not garnered much attention as either a therapeutic or a diagnostic cancer target due to the lack of potent and specific agents.

In accords with our program to discover potent and selective ligands that target various cancers, we have developed two *in vivo* imaging agents that have been successful in murine models (3, 13-18). Figure 1a shows the structure of these agents; the bisaryl urea **1**-Cy5.5 (LLP2A-Cy5.5; Ref. 3 and 15) and the benzothiazole analogue **2**-Cy5.5 (KLCA14-Cy5.5; Ref. 16) both showed high affinity and specificity for B- and T-cell lymphomas containing activated $\alpha_4\beta_1$ integrin, with the latter showing improved tumor:kidney signal. This is likely due to the improved solubility of 2-arylamino azole

heterocycle (14, 16) over the bisaryl urea as these heterocycles have a lower log*P*, a higher dipole moment, and an increased acidity of the 2-arylamino N-H (pK_a = 5.5-6.5; Ref. 19). However, both **1**-Cy5.5 and **2**-Cy5.5 have approximately one third of the molecular weight committed to the $\alpha_4\beta_1$ integrin-targeting motif with the rest of the molecular weight devoted to the linker and the dye. Furthermore, due to the limited range of tissue penetration, optical imaging is not practical for whole-body imaging in human. There is a need to develop a condensed $\alpha_4\beta_1$ integrin radio-targeting agent that not only can be used for PET and SPECT imaging but also for radiotherapy. With efforts integrating heterocyclic chemistry, cell adhesion assays, molecular modeling, and radiochemistry, we report herein the discovery of the bromobenzimidazole carboxamide **5** (IC_{50} = 115 pM), the structure-activity relationship (SAR) between halobenzimidazole carboxamides **3-6**, and the biological evaluation of radio-iodinated derivates **7**, **8** and **18**.

Materials and Methods

Chemical synthesis. Compounds **3-9**, **11-13**, and **16-17** were synthesized as outlined in Supplementary Schemes 1-4. Compounds **1-2** (as well as **1**-Cy5.5 and **2**-Cy5.5), **9**, **14**, and **15a-b** were previously reported (3, 14, 16, 20). The synthesis of **3-6** was analogous to our previous work (16), however the analytical data for these compounds is listed below. The synthesis of **7-8**, **10-13**, and **16**-**21** is described below.

(*S*)-6-(1-Carbamoylcyclohexyl-amino)-5-[(*S*)-2-{4-(5-fluoro-1*H*-benzo[*d*]imidazol-2-yl)amino)-benzamido]-6-[(*E*)-3-(pyridin-3-yl-acrylamido}hexanamido]-6-oxo-hexanoic Acid (3). Following our procedure for benzimidazole analogues (16) afforded **3** as a white solid (10 mg, 44%): ESI-MS (*m/z*) 798.8 $(M+H)^+$, ESI-HRMS for $C_{41}H_{49}FN_9O_7$ $(M+H)^+$: Calcd, 798.3733; found, 798.4481 (*m/z*). Purity was determined to be 96% as determined by analytical HPLC.

(*S*)-6-(1-Carbamoylcyclohexylamino)-5-[(*S*)-2-{4-(5-chloro-1*H*-benzo[*d*]imidazol-2-ylamino)-benzamido]-6-[(*E*)-3-(pyridin-3-yl)acrylamido}hexanamido]-6-oxo-hexanoic Acid (4). Following our procedure for benzimidazole analogues (16) afforded **4** as a white solid (22 mg, 57%): ESI-MS

814.3, 816.3 (*m/z*) $(M+H)^+$, ESI-HRMS for $C_{41}H_{49}ClN_9O_7$ $(M+H)^+$: calcd, 814.3438 found, 814.2894 (*m/z*). Purity (HPLC): 96%.

(*S*)-5-[(*S*)-2-{4-(5-Bromo-1*H*-benzo[*d*]imidazol-2-ylamino}benzamido]-6-[(*E*)-3-(pyridin-3-yl)-acrylamido}hexanamido]-6-(1-carbamoylcyclohexylamino)-6-oxo-hexanoic Acid (5). Following our procedure for benzimidazole analogues (16) afforded **5** as a white solid (28 mg, 39%): ESI-MS (*m/z*) 858.4, 860.6 $(M+H)^+$, ESI-HRMS for $C_{41}H_{49}BrN_9O_7$ $(M+H)^+$: calcd, 906.2794; found, 906.2843 (*m/z*). Purity (HPLC): 99%.

(*S*)-6-(1-Carbamoylcyclohexylamino)-5-[(*S*)-2-{4-(5-iodo-1*H*-benzo[*d*]imidazol-2-ylamino)benz-amido]-6-[(*E*)-3-(pyridin-3-yl)acrylamido}hexanamido]-6-oxohexanoic Acid (6). Following our procedure for benzimidazole analogues (16) afforded **6** as a white solid (18 mg, 48%): ESI-MS 906.3 (*m/z*) $(M + H)^+$, ESI-HRMS for $C_{41}H_{49}IN_9O_7$ $(M + H)^+$: Calcd, 906.2794; Found, 906.2843 (*m/z*). Purity (HPLC): 96%.

[^{125}I]-(*S*)-6-(1-Carbamoylcyclohexylamino)-5-[(*S*)-2-{4-(5-iodo-1*H*-benzo[*d*]imidazol-2-ylamino)-benzamido]-6-[(*E*)-3-(pyridin-3-yl)acrylamido}hexanamido]-6-oxo-hexanoic Acid (7). Radioiodinating of compound bromobenzimazole carboxamide **5** using $Na^{125}I$ was evaluated by a number of methods and conditions but the following procedure provided the most consistent and best yields. Briefly, 50 µL of a 2.5 mM solution of compound **5** in 1 M sodium phosphate (pH 7.0) were added to 50 µL 5 M solution of chloramine-T in distilled water and mixed in a vial containing 185 MBq of $Na^{125}I$ and 10 mol % of CuI at 50 ºC for 20 min. This mixture was then quenched with 100 µL of 5 mM sodium bisulphite for about 15 min. Radiolabeled **7** was eluted through C_{18} spin column with 250 µL of 1:1 acetonitrile/water. Radiolabeling yields were in range of 20-25%, with specific activities ranging from 25.4 to 38.0 MBq (0.8–1.2 µCi)/µmol (specific activity was calculated and corrected after final purification). Quality assurance of the compound **7** was estimated by reverse-phase HPLC with radioactive and UV detectors and the labeled peptide showed a single peak of >95% purity. The final purified products showed >95% monomeric compounds by C_{18} TLC, reverse-phase HPLC and CAE runs of 11 and 45 min; the unbound radioiodine was <5%.

[^{125}I]-(*S*)-6-[1-{(*S*)-3-Amino-2-(4-hydroxy-3-iodobenzyl)-3-oxopropanoyl-carbamoyl}cyclohexylamino]-5-[(*S*)-2-{4-(5-bromo-1*H*-benzo[*d*]imidazol-2-ylamino)benzamido]-6-[(*E*)-3-(pyridin-3-yl)-acrylamido}hexanamido]-6-oxohexanoic Acid (8). A 2.5 mM solution of compound **5** (200 μg, 50μL) in 1 M Na_3PO_4 (pH 7.0) was added to 50 μL of a 5 mM solution of chloramine-T in DMSO (200 μL) and mixed in a vial containing $Na^{125}I$ (1 mCi, 10 μL), 10 mol % diethyldiamine and 10 mol % ratio of CuI at 50 ºC for 20 min. After 20 min this mixture was quenched with 100 μL of a 5 mM $NaHSO_4$ for 15 min. Crude radiolabeled **8** was eluted through C-18 spin column with 250 μL of 1:1 acetonitrile/water to afford pure **8** in 90% radiochemical yield, with specific activities ranging from 25.4 to 38.0 MBq (2 μCi)/μg, and >95% purity. The final purified products showed >95% monomeric compounds by C-18 TLC, RP-HPLC and CAE runs of 11 and 45 min; the unbound radioiodine was <5%.

General Procedure for Halobenzimidazole Acids: 4-(5-Fluoro-1*H*-benzo[*d*]imidazol-2-ylamino)benzoic Acid (10): Our previously reported methods (16) were used with the following exceptions: A sealable microwave tube was used as the reaction vessel and after the consumption of **9** as determined by TLC, 1,3-diisopropylcarbodiimide (451 µL, 2.90 mmol) was added, the tube was sealed, and the reaction mixture was microwave heated to 80 ºC for 11 min. After our previously described workup, this crude ester was then dissolved in DMF (8 mL), transferred to a sealable microwave tube, treated with $Ba(OH)_2$ (1.65 g, 9.65 mmol), and microwave heated to 140 ºC for 21 min. The previously described filtered to afford **10** (225 mg, 86%) as a gray solid: ESI-MS (*m/z*) 272 $(M+H)^+$; Purity (HPLC): 98%.

4-(5-Chloro-1*H*-benzo[*d*]imidazol-2-ylamino)benzoic Acid (11). Following the General Procedure for Halobenzimidazole Acids afforded **11** as a gray solid (249 mg, 89%): ESI-MS (*m/z*) 288, 290 $(M+H)^+$; Purity (HPLC): 99%.

4-(5-Bromo-1*H*-benzo[*d*]imidazol-2-ylamino)benzoic Acid (12). Following the General Procedure for Halobenzimidazole Acids afforded **12** as a gray solid (205 mg, 64%): ESI-MS (*m/z*) 332, 334 $(M+H)^+$; Found C, 50.70; H, 3.03; N, 12.63. Purity (HPLC): 100%.

4-(5-Iodo-1*H*-benzo[*d*]imidazol-2-ylamino)benzoic Acid (13). Following the General Procedure for Halobenzimidazole Acids afforded **13** as a brown solid (275 mg, 75%): ESI-MS (*m/z*) 380.0 $(M+H)^+$; Purity (HPLC): 97%.

(*S*)-6-[1-{(*S*)-3-amino-2-(4-hydroxybenzyl)-3-oxopropanoylcarbamoyl}cyclohexyl-amino]-5-[(*S*)-2-{4-(5-bromo-1*H*-benzo[*d*]imidazol-2-ylamino)benzamido]-6-[(*E*)-3-(pyridin-3-yl)acrylamido}-hexanamido]-6-oxohexanoic Acid (17). Our previously reported methods (22) afforded first **16** and then **17** as a yellow solid (6 mg, 4.9%): ESI-MS 1023.69 (*m/z*) $(M + H)^+$. Purity (HPLC) 91%.

[^{125}I]-(*S*)-6-[1-((*S*)-1-amino-6-(4-iodobenzamido)-1-oxohexan-2-ylcarbamoyl)-cyclohexyl-amino]-5-[(*S*)-2-(4-(5-bromo-1*H*-benzo[*d*]imidazol-2-ylamino)benz-amido]-6-[(*E*)-3-(pyridin-3-yl)acrylamido)hexanamido]-6-oxohexanoic acid (18). Amine **21** (50 μg, 41.2 μmol) and *N*-succinimidyl-4-[^{125}-I]iodobenzoate (14 μg, 41.2 μmol, 200 μCi; Ref 45) in alkaline water (pH 8.0) was warmed to 60 ˚C for 1 h. Crude **18** was eluted through C_{18} spin column with 250 μL of 1:1 acetonitrile/water to afford pure **18** in 47% radiochemical yield, with a specific activity 1.7 μCi/g, and >95% purity. Purity (C_{18} TLC and RP-HPLC): >90%.

(*S*)-5-((*S*)-2-(4-(5-bromo-1*H*-benzo[*d*]imidazol-2-ylamino)benzamido)-6-((*E*)-3-(pyridin-3-yl)acrylamido)hexanamido)-6-(1-((*S*)-1,6-diamino-1-oxohexan-2-ylcarbamoyl)cyclohexylamino)-6-oxohexanoic acid (21). Our previously reported methods (16) afforded **21** (4.9 mg, 4.2%) as a white powder: ESI-MS 988.46 (*m/z*) $(M + H)^+$. Purity (HPLC): 100%.

Multiple Sequence Alignment and Model Building. The sequence alignment between $\alpha_4\beta_1$ integrin and the template ($\alpha_{IIb}\beta_3$ integrin (21), see Supplementary Figures 3-4) was performed using PSI-BLAST-ISS (22). Sequences having similarity to both $\alpha_4\beta_1$ and $\alpha_{IIb}\beta_3$ integrins were used as seeds to generate corresponding PSI-BLAST profiles (23) which were extracted and compared. Protein models were generated using MODELLER (24).

Docking simulations. Compounds were docked in the vicinity of Trp188 in (α_4) using Autodock (25). The partial atomic charges for the ligands were obtained using the AM1-BCC (26) method and

united atom charges were used for the integrin (27). An 80×90×90 grid was used with a spacing of 0.375 Å and centered above Trp188. A Lamarckian algorithm was used to generate ligand conformations using previously reported parameters while keeping the energy evaluations at a maximum of 150,000 (28). A total of 5,000 conformers were generated for each ligand and clustered using a 2.0 Å RMSD.

Cell Adhesion Assay. The cell adhesion assay method is described elsewhere (14, 16).

Animal Biodistribution Study for 7. Eleven female BALB/c nu/nu mice, 5-6 weeks old (UC Davis animal care facility), were xenografted s.c. in the abdomen with 5×10^6 Raji cells. Three weeks after inoculation, the tumor size of the mice was measured. The mice were injected i.v. with 4-6 μCi of ^{125}I-labeled **7** (5 μg, 6 nmol) with normal saline as the vehicle. The mice were sacrificed at 4, 24 and 48 h post injection and tissue samples were excised. The tissue samples were weighed and radioactivity was measured in a γ-counter. Uptake in harvested organs was expressed as % ID/g of tissue.

Animal Biodistribution Study for 18. Six female BALB/c nu/nu mice, 5-6 weeks old (UC Davis animal care facility), were xenografted s.c. in the abdomen with 6×10^6 Raji cells. Three weeks after inoculation, the tumor size of the mice was measured. The mice were injected i.v. with **18** (5 μg, 4 nmol, 12 μCi specific activity) with normal saline as the vehicle. Three mice were sacrificed at 24 h post injection and the other three at 48 h post injection, and tissue samples were excised. The tissue samples were weighed and radioactivity was measured in a γ-scintillation counter. Uptake in harvested organs was expressed as % ID/g of tissue.

Results and Discussion

Chemistry. Both the azole carboxamide and bromoazole acetamide series were previously known to be ineffective ligands for $\alpha_4\beta_1$ integrin. Indeed, previous SAR studies found that a methylene unit between the amide and the phenyl ring (i.e., arylacetamide) was believed to be a critical motif for potency (3) while bromo substitution was ineffective at increasing potency (14, 16). Nonetheless, molecular modeling studies revealed a channel near the ligand binding site where a halogen atom could

potentially interact (16). Halogenated ligands are all particularly attractive for use in medicine and biology as either a radiodiagnostic (^{18}F), a radiotherapeutic (^{131}I), or a molecular structure tool (Cl or Br). In the latter example, either chloro or bromo ligands could be utilized to provide valuable molecular insight into the integrin structure in either photoaffinity cross-linking/mass spectroscopy experiments (Cl, 3:1 ^{35}Cl:^{37}C; Br, 1:1 ^{79}Br:^{81}Br), as well as co-crystallization X-ray studies (heavy atom effect). This provided the impetus behind the synthesis of halobenzimidazole analogues **10-13** (Supplementary Scheme 1).

While milder tandem reactions have been recently developed to afford *m*- and *p*-azole esters in good yields (29, 30), the reaction conditions shown in Supplementary Scheme 1 quarter the amount of time to deliver halobenzimidazole acids **10-13** through microwave-mediated chemistry (31). Briefly, commercially available aniline esters were treated with thiophosgene to afford the aryl isothiocyanate ester **9** in 83% yield. Following purification by short path column chromatography, this aryl isothiocyanate ester was reacted with 4-halo-*o*-phenylenediamine to yield an intermediate bisaryl thiourea that, in the presence of 1,3-diisopropylcarbodiimide (DIC), was cyclized to yield crude benzimidazole esters and 1,3-diisopropylthiourea as a by-product. These esters are rapidly saponified to afford halobenzimidazole acids **10-13** (64-89% yield) that are analytically pure following acidification and filtration (32). This streamlined route, coupled with previous reports focusing on milder reagents and conditions that minimize purification (16, 29), significantly improves the preparation of these medicinally-pertinent azole heterocycles which are present in nearly one-quarter of the top 100 drugs (33).

With these halobenzimidazole acids in hand, effort was then directed towards the synthesis of target molecules **3-6** (Supplementary Scheme 2). The tripeptide **14**, prepared previously from Rink amide resin (14), was *N*-acylated with halobenzimidazole acid precursors **10-13**, followed by acid-mediated deprotection and resin cleavage to afford crude **3-6**. Purification by reverse-phase HPLC and lyophilization delivered pure halobenzimidazole carboxamide analogues **3-6** in 22-46% overall yield from Rink amide resin.

***In Vitro* Biological Evaluation.** Halobenzimidazole carboxamide analogues **3-6** were then subjected to cell adhesion competitive inhibition assays to determine *in vitro* activity and potency. Lusinskas reported that $\alpha_4\beta_1$ integrin mediates cell adhesion to vascular cell adhesion molecule-1 (VCAM-1; CD106) and the extracellular matrix protein fibronectin. The 25-mer peptide CS-1 (DELPQLVTLPHPNLHGPEILDVPST), the binding motif of fibronectin to $\alpha_4\beta_1$ integrin, provides a natural ligand to measure the binding affinities (IC_{50}) of the halobenzimidazole carboxamide analogues **3-6**.

Briefly, 96-well plates were coated with neutravidin followed by treatment of biotinylated CS-1 to immobilize the natural ligand to the well of the plate. The remaining non-neutravidin bound sites were blocked with BSA and the wells were incubated with Molt-4 cells (human T-cell leukemia; contains $\alpha_4\beta_1$ integrin). The plates were then washed, fixed with formalin, stained with crystal violet, and the absorbance (570 nm) was measured using a UV/Vis spectrophotometer equipped to read 96-well plates. Inhibition was calculated as a percentage resulting from the concentration-dependent curve (see Supplementary Materials), with the potency of **3-6** shown in Figure 2a. While all compounds have an affinity for $\alpha_4\beta_1$ integrin at <5 nM, these data suggest that the type of halogen atom plays a critical role for ultrapotency in this class of halobenzimidazole analogues. The bromo, fluoro, and iodo derivatives are particularly promising; the bromo compound **5** is only 2-fold less potent than previous leads (4, 20), while the fluoro (**3**) and iodo (**6**) analogues could potentially be highly potent radiodiagnostic (F-18) and radiotherapeutic (I-131) agents.

SAR and Theoretical Calculations. Interestingly, the SAR for this class of benzimidazole carboxamides (see Figure 2a) revealed that both the unsubstituted benzimidazole (**15a**; Ref. 14) and 5^6-methylbenzimidazole (**15b**; Ref. 16) were 1000-fold less potent than fluoro, chloro, and bromo analogues **3-5** as well as 100-fold less potent than iodo analogue **6**. These data suggest that hydrophobic interactions were not responsible for ultrapotency, as both **15a** and **15b** were equipotent. Additionally, steric interactions were also not responsible, as 1000-fold difference was seen between isosteres **15a** and **3** as well as **15b** and **4**. Electrostatic interactions were also examined; however these interactions were

not important as the electrostatic potential of **3-6** and **15a-b** (see Figure 2b) did not correlate with the observed potency. Therefore, attention turned towards aryl halide-derived interactions which have occurred in prior systems through aryl halide-H-bonding (34) or halogen- carbonyl dipole-dipole interactions (35, 36).

To further understand if aryl halide-H-bond and/or dipole-dipole interactions were involved, the binding energy (E_{bind}) was estimated for **3-6** (see Figure 2a) using the equation $E_{bind} = RT$*ln[IC_{50}(**X** = halogen)/IC_{50}(**X** = H)], where R is the gas constant and T is the temperature at 25 ºC. Quantum mechanical calculations were performed where halobenzimidazoles interacted with primary amide (i.e., Asn/Gln), ammonium (Lys), or carboxylate (Asp/Glu) side chains. Interestingly, only calculations involving the interaction between the primary amide side chain of Asn or Gln with halobenzimidazoles gave results consistent with the experimental observations, thereby eliminating Lys, Asp, and Glu residues as well as charge-transfer interactions. These data suggest that the nature of either the H-bond donor or carbonyl source is critical for ultrapotency.

The nature of the amide-aryl halide interaction was elucidated by investigating the geometries and interaction energies of both the carbonyl oxygen and the amide N-H interacting with the halobenzimidazole. Having the hydrogen N-H interacting with the halogen gave a stabilizing interaction for halobenzamidazoles **3-6**. While the carbonyl oxygen interacting with heavier halo analogues **4-6** was stabilizing, it was unfavorable when interacting with fluoro analogue **3**. The gas-phase calculated interaction energies (*IE*) were then determined at the MP2/6-311++G(d,p)//B3LYP/6-311++G(d,p) level and ranged from 3.5 to 4.0 kcal/mol as shown in the chart of Figure 2a. These *IE* values were primarily due to the H-bond between the primary amide of Asn161 (α_4 subunit) and the halobenzimidazole moiety. The *IE* values predict the fluoro analogue **3** would be the most potent, however all *IE* values are very close (within 0.5 kcal/mol) and are comparable to experimentally observed E_{bind} values. The variation in potency is likely explained by bromo analogue **5** having the halogen with the requisite van der Waal's atomic radii (2.00 Å for Br; Ref. 37) and positioning of the halogen atom (105.8 °; angle of the C(O)NRH···X-Ar H-bond, where X is the central atom of the angle

and a halogen, is taken from the minimized energy structures shown generically in Figure 2a) allowing for this key amide-halogen H-bond (bond length between H···X = 2.87 Å) while permitting other moieties to interact with the α_4 and β_1 subunits (such as the butanoate-Mg^{2+} interaction at the MIDAS site of the β_1 subunit; Ref. 16). This theory helps explain why the larger iodo analogue **6** (the poorest H-bond acceptor) is approximately 10-fold less potent than the fluoro (**3**), chloro (**4**), and bromo (**5**) analogues and 100-fold more potent than the unsubstituted (**15a**) and methyl analogues (**15b**).

Radioiodination via Aromatic Finkelstein and Initial Biodistribution Studies. The condensed radioiodide derivatives **7** and **8** were attractive targets to potentially serve as therapeutic or diagnostic agents for T- and B-cell lymphomas. Buchwald's copper(I)-mediated aromatic Finkelstein reaction with cold sodium iodide (i.e., ArBr□ArI) that proceed with average yields of 97% for many aryl and heteroaryl systems seemed a highly promising route to deliver the I-125 enriched **7** from the aryl bromide **5** (Supplementary Scheme 3; Ref. 38). In our hands, this method for radiohalogenation was unsuccessful, presumably due to the structural sophistication of **5** with several potential heteroatoms available for copper chelation. However, treatment of **5** with [^{125}I]NaI/chloramine-T successfully delivered **7** with a radiochemical yield of 20% and a specific activity of 1.0 μCi/μg (^{125}I $T_{1/2}$ = ~60 d).

Concurrently, Raji cells (human B-cell lymphoma) which abundantly express $\alpha_4\beta_1$ integrin (17), were cultured, centrifuged, and injected into eleven female BALB/c nude mice. These xenograft tumors were allowed to grow to 50-200 mm. The I-125 analogue **7** was then tail vein injected, with animals sacrificed and organs and tumors removed, weighed and counted after 24 and 48 h. Although only one dose formulation was given and dose injections were performed at the same time in an identical manner for all mice, the blood clearance and biodistribution data allowed us to separate the mice into two groups: one with slow blood clearance and one with fast blood clearance (Supplementary Fig. S1 and S2). Three mice showed slow clearances (2 mice at 24 h and 1 mouse at 48 h). These mice had approximately 15% still circulating in the blood thus providing high tumor uptakes of greater than 6% ID/g. The liver, spleen and marrow uptakes were less than 8% ID/g at 48 h. However, five mice (3

mice at 24 h and 2 mice at 48 h) showed that **7** was cleared rapidly from the blood and body. The major dose (25% ID/g) was mainly accumulated in liver, spleen and marrow, while the tumor uptake of these mice was very low (less than 1.5% ID/g).

While these preliminary data have low statistical significance, we believe these results warrant further discussion and may be due to one or more factors. The radioiodo analogue **7**, having reduced *in vitro* affinity for $\alpha_4\beta_1$ integrin by nearly ten-fold compared to the bromo analogue **5**, may have decreased *in vivo* affinity and selectivity. The iodobenzamidyl moiety of **7** may also be metabolically degraded, as seen with *p*-radioiodobenzamide derivatives (39, 40). While we did not see *in vitro* peptide aggregation of **7**, it has been reported that the fast clearance patterns may be due to *in vivo* aggregation resulting in ineffective tumor targeting (41).

Radioiodination via Electrophilic Aromatic Substitution. In addition to these mixed *in vivo* results (Supplementary Figs. S1 and S2), **7** was difficult to prepare in high radiochemical yield and crude purity. This provided impetus for the synthesis of 3-radioiodotyrosine-derivative **8**, as tyrosine residues are rapidly radioiodinated with high regio- and chemoselectively (42, 43). Moreover, previous optical conjugates **1**-Cy5.5 and **2**-Cy5.5 showed that the primary amide is successfully modified to a secondary amide without affecting activity, potency, or selectivity (3, 13, 15-17). With this in mind, Rink amide resin was first swollen in DMF for 3 h, followed by Fmoc-deprotection and *N*-acylation with semi-orthogonally protected tyrosine to deliver the tyrosylated resin **16** (Supplementary Scheme 2). This resin was further elaborated into the bromobenzimidazole tetrapeptide **17** through analogous chemistry (Supplementary Scheme 2) and further elaborated elsewhere (20). This tyrosine derivative **17** was then rapidly radioiodinated using I-125 enriched sodium iodide with iodogen as an oxidant to afford the 3-radioiodo tyrosine derivative **8** in 90% radiochemical yield and with a specific activity of 2 μCi/μg. Unfortunately, **8** performed poorly in *in vitro* binding studies (<4%) and thus *in vivo* studies were not pursued. However, these *in vitro* results should not necessarily be viewed detrimentally; the *o*-hydroxyl

group has been known to weaken the carbon-iodine bond and radioiodotyrosine derivatives have been known to undergo *in vivo* degradation due to their structural similarities to thyroid hormones (44).

Radioiodination via Succinimidyl Ester Chemistry and Biodistribution Studies. Attention was then turned towards the synthesis of 4-radioiodobenzamidolysine-derivative **18**, as the bulkiness of the iodotyrosine may contribute to the poor *in vitro* binding. Rink amide resin was first swollen in DMF for 3 h, followed by Fmoc-deprotection and *N*-acylation with Fmoc-Lys(Dde)-OH to deliver resin **19** (Figure 3). Resin **19** was further elaborated into resin **20** through analogous chemistry (Supplementary Scheme 2) and described elsewhere (16). *N*-acylation of **20** with Fmoc-Lys(Alloc)-OH was followed by Fmoc-deprotection, and then coupling with bromobenzimazole acid **5**. Alloc deprotection, followed by *N*-acylation with *trans*-3-(3-pyridyl)acrylic acid, Dde deprotection, and TFA cleavage yielded **21**. The lysinated bromobenzimadole **21** was radioiodinated by coupling the free amine of the lysine with the NHS-ester of I-125 enriched 4-iodobenzoic acid (prepared from *p*-aminobenzoic acid as outlined by Khalaj et al.; Ref. 45) to afford the 4-radioiodobenzamidolysine derivative **18** in 47% radiochemical yield and with a specific activity of 1.7 μCi/μg.

To study the preliminary biodistribution of **18**, Raji cells (human B-cell lymphoma) expressing $\alpha_4\beta_1$ integrin were cultured, centrifuged, and injected into six nude mice. These xenograft tumors were grown to 50-200 mm. The I-125 analogue **18** was then tail vein injected, with half of the animals being sacrificed after 24 h and 48 h. As shown in Figure 4, the organs and tumors were removed and counted with **18** having good tumor uptake (12 $\pm$ 1% ID/g at 24 h and 4.5 $\pm$ 1% ID/g at 48 h) and minimal uptake in other organs. In particular, the low kidney uptake (tumor:kidney$_{(t = 24h)}$ ~4:1; tumor:kidney$_{(t = 48h)}$ ~2.5:1) was encouraging as this, in this initial assessment, has demonstrated that radio-labeled azole anologue **18** may be a promising payload-ligand conjugate for targeting activated $\alpha_4\beta_1$ integrin expressed tumors.

Conclusion

The results presented have demonstrated the importance of advancing leads to target cancerous but not normal cells by exploiting the conformational differences of $\alpha_4\beta_1$ integrin. The synthesis of azole heterocycles, which previously required harsh reaction conditions, long reaction times, and highly toxic reagents, can now be rapidly prepared through microwave-mediated synthesis using safer reagents with minimal purification. This report also provides an excellent example of how molecular models can be used as a guide to predict analogues that will have high affinity and to understand key weak-force interactions. The potency of this unique class of compounds is likely attributed to a key aryl halide-hydrogen bond between the halobenzimidazole moiety and the primary amide side chain of Asn161 in the α_4 subunit. In preliminary studies, the condensed radio-iodobenzimidazole analogue **18** demonstrates that a low tumor:kidney ratio may be achievable with a covalently attached radio-labeled modality while minimizing the size and cost of the payload-ligand conjugate. These halobenzimidazoles are particularly attractive as this allows for the design of highly condensed ligand-payload conjugates for radiotherapeutic (I-131) and radiodiagnostic (F-18) agents for selectively detecting and treating T- and B-cell lymphomas that express $\alpha_4\beta_1$ integrin. Additionally, the bromo analogues **5** could provide valuable molecular insight into the binding site and integrin structure through photoaffinity cross-linking/mass spectroscopy (1:1 ^{79}Br:^{81}Br) as well as co-crystallization X-ray studies (heavy atom effect).

Supplemental Data for this research article is available at Cancer Research Online.

References

1. Hait WN. Targeted cancer therapeutics. Cancer Res 2009;69:1263-7.

2. Shimaoka M, Takagi J, Springer TA. Conformational regulation of integrin structure and function. Annu Rev Biophys Biomol Struct 2002;31:485-516.

3. Peng L, Liu R, Marik J, Wang X, Takada Y, Lam KS. Combinatorial chemistry identifies high-affinity peptidomimetics against $\alpha_4\beta_1$ integrin for *in vivo* tumor imaging. Nat Chem Biol 2006;2:381-9.

4. Martin KH, Slack JK, Boerner SA, Martin CC, Parsons T. Integrin connections map: To infinity and beyond. Science 2002;296:1652-3.

5. Yusuf-Makagiansar H, Anderson ME, Yakovleva TV, Murray JS, Siahaan TJ. Inhibition of LFA-1/ICAM-1 and VLA-4/VCAM-1 as a therapeutic approach to inflammation and autoimmune diseases. Med Res Rev 2002;22:146-67.

6. Vincent AM, Cawley JC, Burthem J. Integrin function in chronic lymphocytic leukemia. Blood 1996;87:4780-8.

7. Marco RA, Diaz-Montero CM, Wygant JN, Kleinerman ES, McIntyre BW. α4 integrin increases anoikas of human osteosarcoma cells. J Cell Biochem 2003;88:1038-47.

8. Matsunaga T, Takemoto N, Sato T, et al. Interaction between leuekmic-cell VLA-4 and stromal fibronectin is a decisive factor for minimal residual disease of acute myelogenous leukemia. Nat Med 2003;9:1158-65.

9. Olson DL, Burkly LC, Leone DR, Dolinsky BM, Lobb RR. Anti-α4 integrin monoclonal antibody inhibits multiple myeloma growth in a murine model. Mol Cancer Ther 2005;4:91-9.

10. Garmy-Susini B, Jin H, Zhu Y, Hwang R, Varner J. Integrin α4β1-VCAM-1-mediated adhesion between endothelial and mural cells is required for blood vessel maturation. J Clin Invest 2005;115:1542-51.

11. Jin H, Su J, Garmy-Susini B, Kleeman J, Varner J. Integrin α4β1 promotes monocyte trafficking and angiogenesis in tumors. Cancer Res 2006;66:2146-52.

12. de la Fuente MT, Casanova B, Garcia-Gila M, Silva A, Garcia-Pedro A. Fibronectin interaction with $\alpha_4\beta_1$ integrin prevents apoptosis in B-cell chronic lymphocytic leukemia: Correlation with Bcl-2 and Bax. Leukemia 1999;13:266-274.

13. Park SI, Manat R, Vikstrom B, et al. The use of one-bead one-compound combinatorial library method to identify peptide ligands for $\alpha_4\beta_1$ integrin receptor in non-Hodgkin's lymphoma. Lett Pept Sci 2002;8:171-8.

14. Carpenter RD, Andrei M, Lau EY, et al. Highly potent, water soluble benzimidazole antagonist for activated $\alpha_4\beta_1$ integrin. J Med Chem 2007;50:5863-7.

15. Peng L, Liu R, Andrei M, Xiao W, Lam KS. In vivo optical imaging of human lymphoma xenograft using a library-derived peptidomimetc against $\alpha_4\beta_1$ integrin. Mol Canc Ther 2008;7:432-7.

16. Carpenter RD, Andrei M, Lau EY, et al. Selectively targeting T- and B-cell lymphomas: A benzothiazole antagonist for $\alpha_4\beta_1$ integrin. J Med Chem 2009;52:14-9.

17. DeNardo SJ, Liu R, Albrect H, et al. ^{111}In-LLP2A-DOTA polyethylene glycol-targeting α4β1 integrin: Comparative pharmacokinetics for imaging and therapy of lymphoid malignancies. J Nucl Med 2009;50:625-34.

18. For a recent review, see: Aina OH, Liu R, Sutcliffe JL, Marik J, Pan C-X, Lam KS. From combinatorial chemistry to cancer-targeting peptides. Mol Pharmaceutics 2007;4:631-51.

19. Perkins JJ, Zartman AE, Meissner RS. Synthesis of 2-(alkylamino)benzimidazoles. Tetrahedron Lett 1999;40:1103-6.

20. Katritzky AR, Witek, RM, Rodriguez-Garcia V, et al. Benzotriazole-assisted thioacylation. J Org Chem 2005;70:7866-81.

21. Xiao T, Takagi J, Coller BS, Wang JH, Springer TA. Structural basis for allostery in integrins and binding of fibrinogen-mimetic therapeutics. Nature 2004;432:59.

22. Margelevicius M, Venclovas C. PSI-BLAST-ISS: an intermediate sequence search tool for estimation of the position-specific alignment reliability. BMC Bioinformatics 2005;6:185.

23. Altschul SF, Madden TL, Schaffer AA, et al. Gapped BLAST and PSI-BLAST: a new generation of protein database search programs. Nucleic Acids Res 1997;25:3389.

24. Sali A, Blundell TL. Comparative protein modeling by satisfaction of spatial restraints. J Mol Biol 1993;234:779.

25. Morris GM, Goodsell DS, Halliday RS, et al. Automated docking using a Lamarckian genetic algorithm and an empirical binding free energy function. J Comput Chem 1998;19:1639.

26. Jackalian A, Jack DB, Bayly, CI. Fast, efficient generation of high-quality atomic charges. AM1-BCC model: II. Parameterization and validation. J Comput Chem 2002;23:1623.

27. Weiner SJ, Kollman PA, Case DA, et al. A new force field for molecular simulation of nucleic acids and proteins. J Am Chem Soc 1984;106:765.

28. Legge GB, Morris GM, Sanner MF, Takada Y, Olson AJ, Grynszpan F. Model of the alpha L beta 2 integrin I-domain/ICAM-1 DI interface suggest that subtle changes in loop orientation determine ligand specificity. Proteins: Struc Func Genetics 2002;48:151.

29. Carpenter RD, DeBerdt PB, Lam KS, Kurth MJ. A carbodiimide-based library method. J Comb Chem 2006;8:907-14.

30. Esters in the *o*-position cyclized to the tetracyclic benzimidazoquinazolinone. For more information and an optimized route to this heterocycle, see: Carpenter RD, Lam KS, Kurth MJ. Microwave-mediated heterocyclization to benzimidazo[2,1-*b*]quinazolin-12(5*H*)-ones. J Org Chem 2007;72:284-7.

31. For representative work from this laboratory, see: Carpenter RD, Fettinger JC, Lam, KS, Kurth, MJ. Asymmetric catalysis: Polystyrene-bound hydroxyprolylthreonine in the enamine-mediated preparation of chromanones. Angew Chem 2008;120:6507-10; Angew Chem Int Ed 2008;47:6407-10.

32. These unique heating conditions were obtained from Biotage's microwave conversion chart: http://www.biotage.com/DynPage.aspx?id=21996.

33. Martin EJ, Critchlow RE. Beyond mere diversity: Tailoring combinatorial libraries for drug discovery. J Comb Chem 1999;1:32-45.

34. Lu Y, Wang, Yong W, Xu Z, et al. C-X···H contacts in biomolecular systems: How they contribute to protein-ligand binding affinity. J Phys Chem B 2009;113:12615-21.

35. Auffinger P, Hays FA, Westhof E, Ho PS. Halogen bonds in biological molecules. Proc Natl Acad Sci USA 2004;101:16789-94.

36. For recent aryl iodide interactions with nucleic acids, see: Tawarada R, Seio K, Sekine M. Synthesis and properties of oligonucleotides with iodo-substituted aromatic aglycons: Investigation of possible halogen bonding base pairs. J Org Chem 2008;73:383-90.

37. Peet JH. How big is an atom? Phys Educ 1975:508-510.

38. Klapers A, Buchwald SL. Copper-catalyzed halogen exchange in aryl halides: An aromatic Finkelstein reaction. J Am Chem Soc 2002;124:14844-45.

39. Garg PK, Slade SK, Harrison CL, Zalutsky MR. Labeling proteins using aryl iodide acylation agents: Influence of *meta* vs *para* substitution on *in vivo* stability. Nucl Med Biol 1989;16:669-73.

40. Wilbur DS, Hamlin DK, Chyan M-K, Kegley BB, Quinn J, Vessella RJ. Biotin reagents in antibody pretargeting. 6. Synthesis and *in vivo* evaluation of astatinated and radioiodinated aryl– and *nido*-carboranyl-biotin derivatives. Bioconjug Chem 2004;15:601-16.

41. Yoshimoto M, Ogawa K, Washiyama K, et al. $\alpha_v\beta_3$ Integrin-targeting radionuclide therapy and imaging with monomeric RGD peptide. Intl J Cancer 2008;123:709-15.

42. Fernandes C, Oliveira C, Gano L, Bourkoula A, Pirmettis I, Santos I. Radioiodination of new EGFR inhibitors as potential SPECT agents for molecular imaging of breast cancer. Bioorg Med Chem 2007;15:3974-80.

43. Kersemans V, Cornelissen B, Kersemans K, et al. Comparative biodistribution study of the new tumor tracer [^{123}I]-2-iodo-L-phenylalanine with [^{123}I]-2-iodo-L-tyrosine. Nucl Med Biol 2006;33:111-7.

44. Smallridge RC, Burman KD, Ward KE, et al. 3',5'-Diiodothyronine to 3'-monoiodothyronine conversion in the fed and fasted rat: Enzyme characteristics and evidence for two distinct 5'-deiodinases. Endocrinology 1981;108:2336-45.

45. This was prepared in 4-steps from *p*-aminobenzoic acid using the following protocol: Khalaj A, Beiki D, Rafiee H, Najafi R. A new and simple synthesis of *N*-succinimidyl-4-[$^{127/125}$I]iodobenzoate involving a microwave-accelerated iodination step. J Labelled Cpd Radiopharm 2001;44:235-40.

Figure 1. Structures of: (a) **1**-Cy5.5 (Ref. 4) and **2**-Cy5.5 (Ref. 22); (b) halobenzimidazole analogues **3-7**; (c) The bishalo analogues **8** and **18** which incorporate the bromobenzimidazole moiety and a distal radioiodide.

Figure 2. (a) Potency (IC_{50}), estimated binding energies, calculated interaction energies, and amide-halogen geometries, where the amide represents a nearby primary amide of Asn161 (α_4 subunit) side chain: *a*. see Ref. 20 for more on **15a**, Ref. 22 for more on **15b**; *b*. Energies are expressed in units of

kcal/mol; *c*. estimated binding energies (E_{bind}), where $E_{bind} = RT$*ln[IC_{50}(**X** = halogen)/IC_{50}(**X** = H)]; *d*. Calculated interaction energy for amide-halogen interaction (gas-phase) using MP2/6-311++G(d,p)//B3LYP/6-311++G(d,p) level of theory, second values are the BSSE corrected energies; *e*. Distances for the van der Waal's (vdW) radii of each halogen are expressed in Å; *f*. Distances (in Å) represent the C(O)NRH---XAr H-bond length; *g*. Represents the H-X-Ar angle in the C(O)NRH---XAr H-bond. (b) Electrostatic potential maps for **3-6** and **15a-b**.

Figure 3. Preparation of **18** from the tyrosine derivative **19.**

Figure 4. *Ex vivo* radio-uptake data of **18** for various tumors and organs.

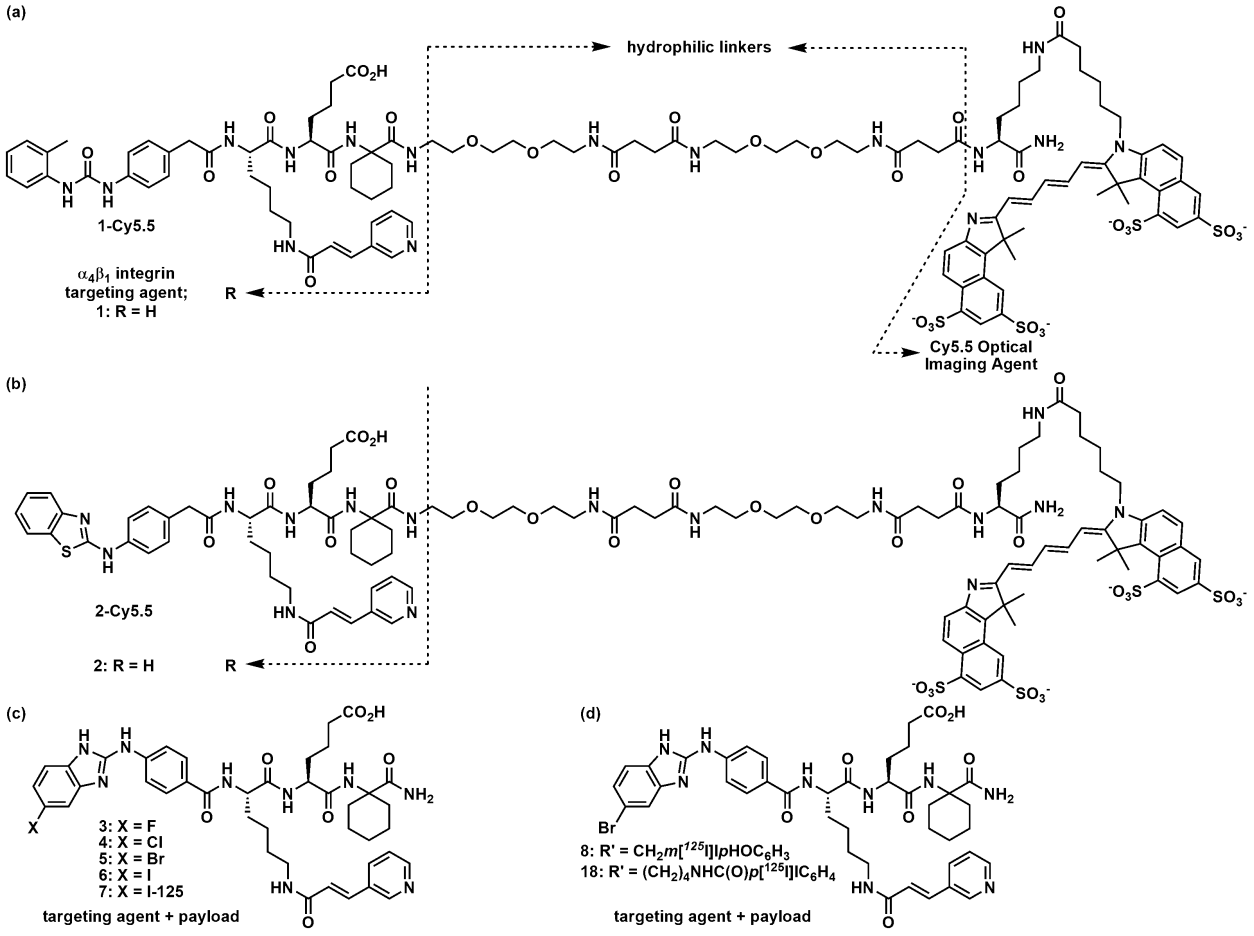
(a)
hydrophilic linkers
1-Cy5.5
$\alpha_4\beta_1$ integrin
targeting agent;
1: R = H
R
Cy5.5 Optical
Imaging Agent
(b)
2-Cy5.5
2: R = H
R
(c)
3: X = F
4: X = Cl
5: X = Br
6: X = I
7: X = I-125
targeting agent + payload
(d)
8: R' = $CH_2m[^{125}I]IpHOC_6H_3$
18: R' = $(CH_2)_4NHC(O)p[^{125}I]IC_6H_4$
targeting agent + payload

Figure 1.

(a)

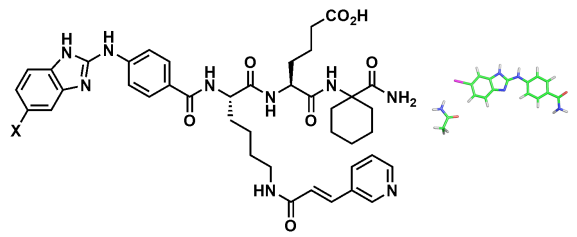

Cpd	X	IC_{50}	E_{bind}[b,c]	IE[b,d]	vdW radii[e]	NH---XAr BL[f]	H---X-C ANG[g]
3	F	657.3 ± 210 pM	-3.98	-4.64,-3.26	1.35	2.13	129.9 °
4	Cl	570 ± 51.6 pM	-4.06	-4.23,-2.53	1.81	2.73	110.4 °
5	Br	134 ± 42.6 pM	-4.95	-4.17,-2.66	2.00	2.87	105.8 °
6	I	3.62 ± 0.3 nM	-2.93	-4.58,-3.05	2.18	3.18	100.8°
15a[a]	H	419 ± 333 nM					
15b[a]	CH_3	490 ± 329 nM					

(b)

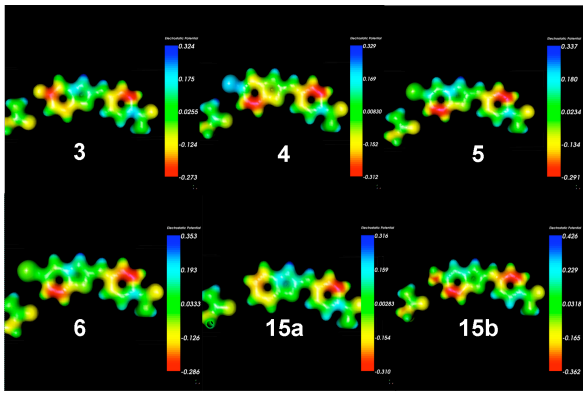

Figure 2.

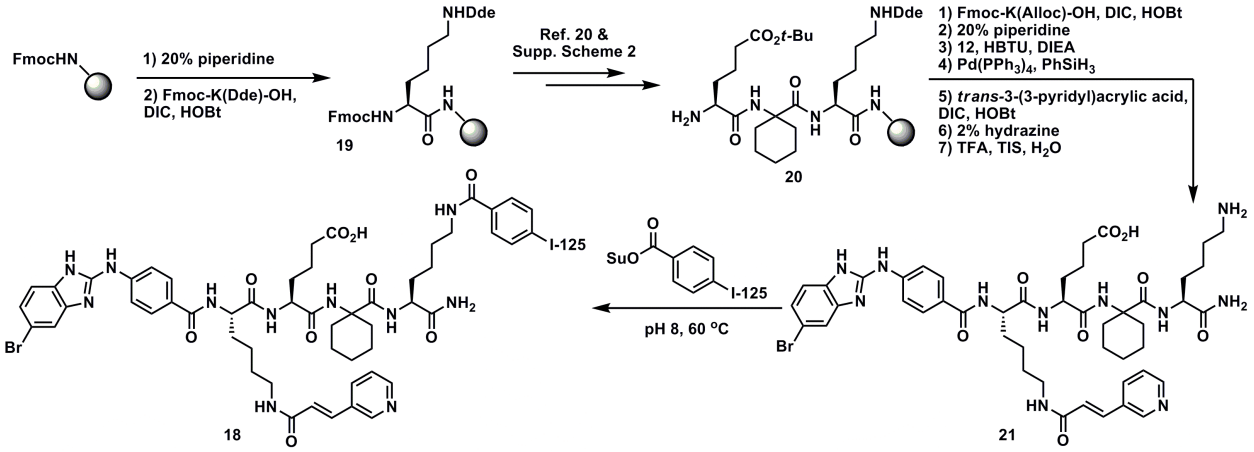

Figure 3.

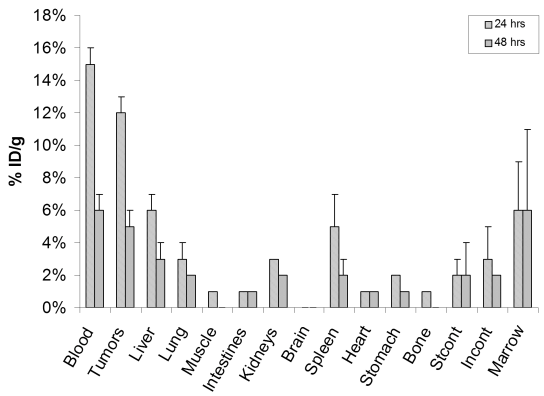

Figure 4.